metals

MDPI

Article

Tunable Complex Permittivity and Strong Microwave Absorption Properties of Novel Dielectric-Conductive ZnO/C Hybrid Composite Absorbents

Junxiao Yan, Hongyao Jia *, Liang Zhou *, Zhenjun Wang and Hongbo Wang *

School of Materials Science and Engineering, Chang'an University, Xi'an 710064, China
* Correspondence: hongyaojia11@163.com (H.J.); zhouliang@chd.edu.cn (L.Z.); wanghb@chd.edu.cn (H.W.)

Abstract: Modern electronic information technology has led social life into inevitable electromagnetic pollution, making microwave absorbing materials more and more important. Herein, dielectric-conductive ZnO/C hybrid composite absorbents were prepared by two-step carbonization with ZnO powders and glucose as critical materials. The electrical conductivity, complex permittivity, and reflection loss were analyzed to study the dielectric and microwave absorption properties. Results show that the prepared ZnO/C composite absorbents exist in the form of rod-like ZnO dispersed in the irregular block carbon, and the complex permittivity of the composite absorbents can be adjusted via varying the carbonization temperature. The minimum reflection loss of −25.64 dB is achieved at 1.8 mm thickness for the composite absorbent with 50 wt.% absorbent content as the final carbonization temperature is 750 °C, and the optimum effective absorption bandwidth is 2.21 GHz at 9.64–11.85 GHz. The excellent microwave absorption properties of ZnO/C composite absorbents are attributed to the combination actions of dipole polarization, conductance loss, and interface polarization, which is significant for the purposeful design of superior microwave-absorbing materials with dielectric and conductive absorbents.

Keywords: carbonization; complex permittivity; dielectric-conductive coupling; microwave absorption; ZnO/C absorbents

check for updates

Citation: Yan, J.; Jia, H.; Zhou, L.; Wang, Z.; Wang, H. Tunable Complex Permittivity and Strong Microwave Absorption Properties of Novel Dielectric-Conductive ZnO/C Hybrid Composite Absorbents. *Metals* **2023**, *13*, 1220. https://doi.org/10.3390/met13071220

Academic Editor: Leonid M. Kustov

Received: 22 May 2023
Revised: 25 June 2023
Accepted: 28 June 2023
Published: 1 July 2023

Copyright: © 2023 by the authors. Licensee MDPI, Basel, Switzerland. This article is an open access article distributed under the terms and conditions of the Creative Commons Attribution (CC BY) license (https://creativecommons.org/licenses/by/4.0/).

1. Introduction

The extensive applications of electromagnetic waves play important roles in the improvement of military and civil electronic equipment [1,2]. However, more attention has also been paid to the electromagnetic interference problems, which not only lead to the failure of electronic device but also endanger the health of humans [3]. Therefore, eliminating or attenuating the incident electromagnetic waves as much as possible has attracted more attention of the researchers all over the world [4,5].

Microwave absorbents have become one of the efficient ways to solve the problems of electromagnetic radiation, which makes them great values in the military and civil fields. Common microwave absorbents include ferromagnetic absorbents, carbon absorbents, ceramic absorbents, etc. Among these candidates, carbon absorbents have attracted extensive attentions due to their low cost, light weight, and favorable electrical conductivity. However, the actual applications of pure carbon materials have been limited because of their intrinsic high electrical conductivity and the resulting impedance mismatch [6]. By comparison, these problems can be efficiently solved by the application of composite absorbents, and a series of studies on carbon series composite absorbents have also been reported [7–9]. Park et al. prepared Fe_3O_4@C composite nanoparticles with yolk-shell structure with the hydrothermal polymerization carbonization method [10]. It was found that the multiple reflections and interfacial polarization effects caused by the core-cavity and cavity-shell interfaces greatly improved the microwave absorption properties. Xu et al. prepared TiO_2/C composite absorbents through a one-step hydrogenation-carbonization

method, and the prepared composite absorbents exhibit excellent microwave absorption properties with the minimum reflection loss of −73.2 dB [11]. Up to now, the composite absorbents with carbon component present favorable electromagnetic characteristics composited with other materials, and it seems to be a much more effective way to adjust the complex permittivity and improve microwave absorption properties.

Recently, the research of carbon series absorbents using biomass materials as carbon sources has attracted extensive attention [12–14]. Among them, glucose [15], sucrose [16], and other biomass materials possess great application potential in the field of microwave absorption due to their low cost, wide sources, and safe chemical components. Wu et al. prepared magnetite dendrite (MDS)/sugar carbon (SC) nanocomposites with sucrose as carbon source and Fe_2O_3 as magnetite precursor, and the optimal reflection loss is −49.90 dB (d = 1.9 mm) [16]. Meanwhile, ZnO has been widely used in the fields of solar cells, photocatalysis, electronics, and gas sensors as a type of dielectric material with simple preparation, controllable structure, and wide band gap (3.37 eV). However, the application of ZnO as microwave absorbent has been limited due to its low electrical conductivity [17,18].

In view of the evident difference in intrinsic dielectric properties between ZnO and carbon materials, dielectric-conductive coupled ZnO/C composite absorbents could not only take advantage of the excellent dielectric characteristics of ZnO but also effectively adjust the impedance matching of carbon materials. Therefore, this study proposes to prepare ZnO/C composite absorbents by a simple two-step carbonization method. Specifically, the composite absorbents were in a negative pressure state to discharge the gas timely in the process of pre-carbonization, and the atmosphere of inert gas was given to improve the critical temperature of the carbothermal reduction reaction during the final carbonization. The thermogravimetric, X-ray diffraction, Raman spectra, X-ray photoelectron spectroscopy, morphology, complex permittivity, and electrical conductivity of the prepared dielectric-conductive coupled ZnO/C composite absorbents with various carbonization temperatures were characterized, and the microwave absorption properties were systematically assessed.

2. Materials and Methods

2.1. Materials

Glucose ($C_6H_{12}O_6$, 99%) and ethylenediamine (EDA, $C_2H_8N_2$, 98%) were purchased from Tianjin Yili Chemical Reagent Factory, Tianjin, China, and Tianjin Damao Chemical Reagent Factory, Tianjin, China, respectively. Zinc nitrate ($Zn(NO_3)_2{\cdot}6H_2O$, 99%) and ethanol were acquired from Tianjin Fengchuan Chemical Reagent Technology Co., Ltd., Tianjin, China, and polyvinyl alcohol (PVA, $[C_2H_4O]_n$, 95%) was supplied by Foshan Shangshan Chemical Co., Ltd., Foshan, China. All the chemicals were analytical grade and used as received.

2.2. Preparation of ZnO Powders

ZnO was prepared by the hydrothermal method. Firstly, 1 g $Zn(NO_3)_2{\cdot}6H_2O$ was added to the deionized water at a concentration of 0.0625 mol/L, and EDA was then added to the $Zn(NO_3)_2$ solution slowly with magnetic stirring, and the molar ratio of Zn^{2+} to EDA was 1:1. Next, the mixed solution was transferred into a reaction tank and held in an oven at 120 °C for 10 h. Following this, the white precipitates were centrifuged and washed for three times with ethanol and deionized water. Finally, the samples were dried, ground, and screened using a 100-mesh screen, and thus the ZnO was obtained.

2.3. Preparation of ZnO/C Composite Absorbents and C Powders

A beaker containing 30 mL polyvinyl alcohol solution with 1 wt.% PVA content was placed on a magnetic stirrer. Then, 8 g glucose powders were added slowly, and continuous stirring of 10 min at 30 °C was performed to fully dissolve the glucose. Subsequently, 0.5 g ZnO was slowly added to the above solution and stirred for 30 min. After that, the

temperature of the solution was raised to 45 °C, and the water was evaporated to obtain the precursor solution.

The precursor solution needs to be cured before carbonization. In the following, the above precursor solution was put into a vacuum oven at 180 °C for 10 h, and the sample was recorded as PZO. Then, the PZO sample was fully ground and placed in the tubular furnace for carbonization treatment. In the pre-carbonization stage, the tubular furnace was vacuum pumped to discharge the gas generated in the reaction process. The heating rate was set at 2 °C/min, and the pre-carbonization temperature and time of all the samples are 400 °C and 60 min, respectively. In the stage of final carbonization, the sample obtained above was carbonized with the heating rate of 5 °C/min in argon atmosphere at 650 °C, 700 °C, and 750 °C. The ZnO/C composite absorbents were mixed with paraffin, and the corresponding paraffin-matrix composite samples filled with 50 wt.% ZnO/C absorbent content were named as CZO50-650, CZO50-700, and CZO50-750, respectively. Meanwhile, the paraffin-matrix composite samples filled with 40 wt.% and 60 wt.% ZnO/C absorbent (carbonized at 750 °C) content were named as CZO40-750 and CZO60-750. In addition, pure glucose was carbonized to obtain carbon powders in the same experimental process. The parameters of carbonization and ZnO/C absorbent content are shown in Table 1, and the synthesis process of the investigated ZnO/C composite absorbents is exhibited in Figure 1.

Table 1. Carbonization parameters of ZnO/C composite absorbents.

Samples	Final Carbonization Temperature (°C)	Final Carbonization Time (min)	Absorbent Content (wt.%)
CZO50-650	650	90	50
CZO50-700	700	90	50
CZO50-750	750	90	50
CZO40-750	750	90	40
CZO60-750	750	90	60

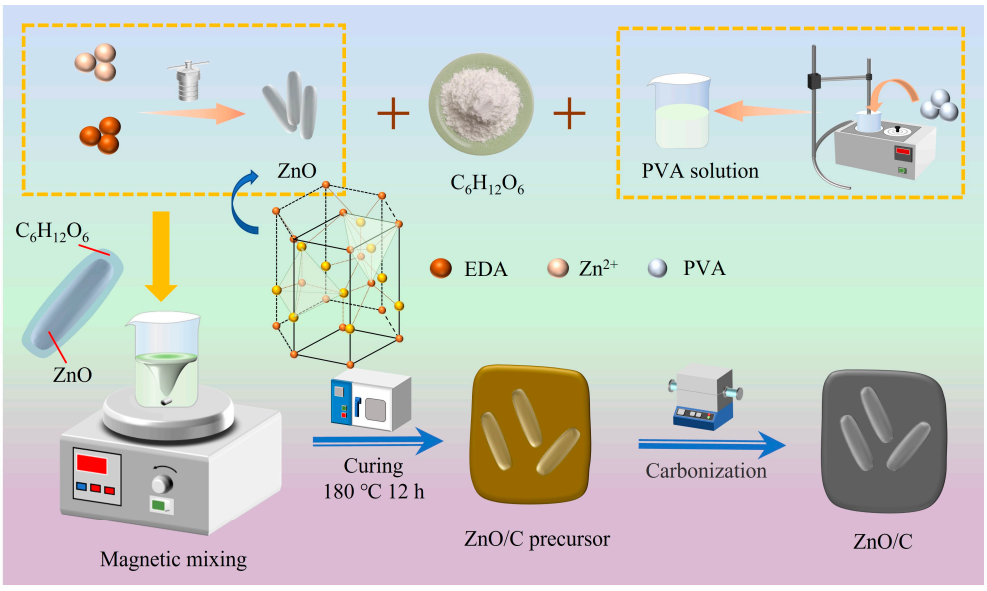

Figure 1. Schematic illustration of the synthesis process of ZnO/C composite absorbents.

2.4. Characterization

The synchronous thermal analyzer (SDT650, TA instruments, New Castle, DE, USA) was used to analyze the thermal stability of the samples. The phase composition was detected by X-ray diffraction (XRD, Bruker AXS D8) using Cu Kα radiation (40 kV, 40 mA) at a scanning speed of 10°/min, and the element composition was further verified by X-ray photoelectron spectroscopy (XPS, K-Alpha+, Thermo Scientific, Waltham, MA, USA). Raman spectroscopy (Nanofider 30) was used to evaluate the samples using hydrogen

ion laser with a wavelength of 632.8 nm. The surface morphology was characterized by scanning electron microscopy (SEM, Hitachi S-4800), and the element distribution was performed by the energy spectrum analyzer (EDS). In addition, the vector network analyzer (E8362B, VNA, Agilent, Palo Alto, CA, USA) was used to measure the complex permittivity in the frequency range of 8.2–12.4 GHz with the sample size of 22.86 × 10.16 × 2.0 mm by the waveguide method. The direct current (DC) conductivity of the samples was tested with a four-probe resistivity tester (HPS2662).

3. Results and Discussion

3.1. Thermogravimetric Analysis

Figure 2 shows the thermogravimetric (TG) and derivative thermogravimetric (DTG) curves of glucose and PZO samples. It can be observed that the TG curve of glucose tends to be flat as the temperature is higher than 404 °C, indicating that the glucose has been well decomposed and carbon products are obtained. In addition, a rapid decline in the quality of PZO between 783 °C and 925 °C can be observed, and the phenomenon can be explained by the carbothermal reduction reaction for our investigated ZnO/C composite absorbents, which is shown in Equation (1) and it is described as follows [19,20]:

$$ZnO_{(s)} + C_{(s)} \xrightarrow{\Delta} Zn_{(g)} + CO_{(g)} \quad (1)$$

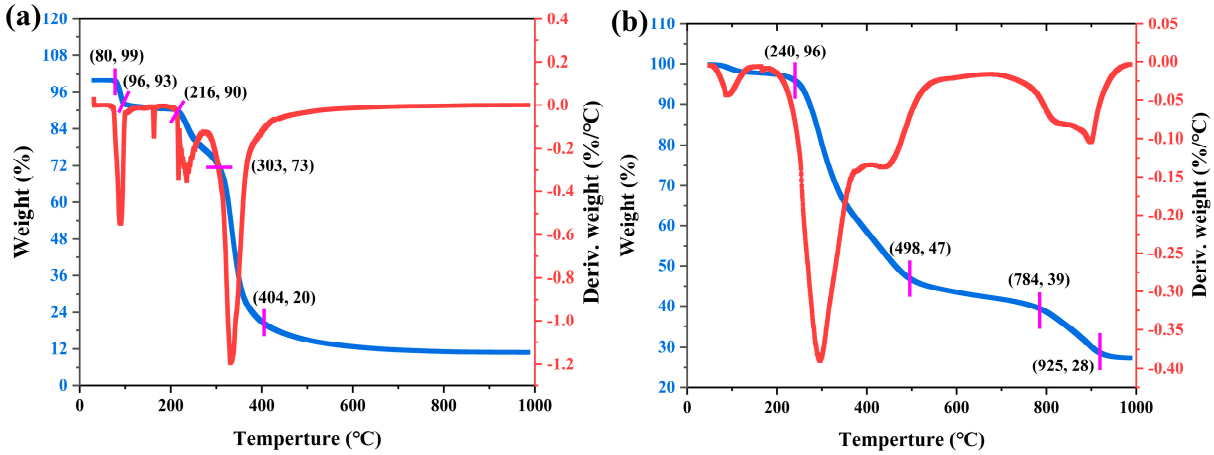

Figure 2. TG curve (blue) and DTG curve (red) of (**a**) the glucose and (**b**) the PZO sample.

Moreover, the content of residual PZO is 25 wt.% as the temperature is higher than 925 °C, which is much higher than that of the carbon products (12 wt.%) obtained after the pyrolysis of glucose, indicating the existence of ZnO in the sample.

3.2. XRD, Raman, and XPS Spectrum Analysis

Figure 3a–c shows the XRD patterns of ZnO/C composite absorbents with different final carbonization temperatures in the angular range from 10°–80°, 10°–30°, and 38°–46°, respectively. As shown in Figure 3a, the XRD curves of the samples cured at 180 °C and pre-carbonized at 400 °C met the standard characteristic peaks of ZnO (JCPDS No. 36-1451). Meanwhile, the diffraction peaks of ZnO could also be observed in the samples obtained by the final carbonization temperature of 650 °C, 700 °C, and 750 °C. However, the intensity of ZnO diffraction peaks increases firstly and then decreases with the increase in carbonization temperature. In addition, a large amount of organic matter for the samples cured at 180 °C and pre-carbonized at 400 °C can be observed in terms of the wide diffraction peak at 2θ = 19.77° and 2θ = 13.04°. As shown in Figure 3b,c, the wide diffraction peaks corresponding to (002) and (100) of the samples after two-step carbonization treatment can be observed, and they belong to amorphous carbon [21–23]. Furthermore, the diffraction peak intensity of the sample at (002) and (100) crystal planes increases evidently with the

increase in the final carbonization temperature, which can be attributed to the increase in the graphitization degree for the carbon products.

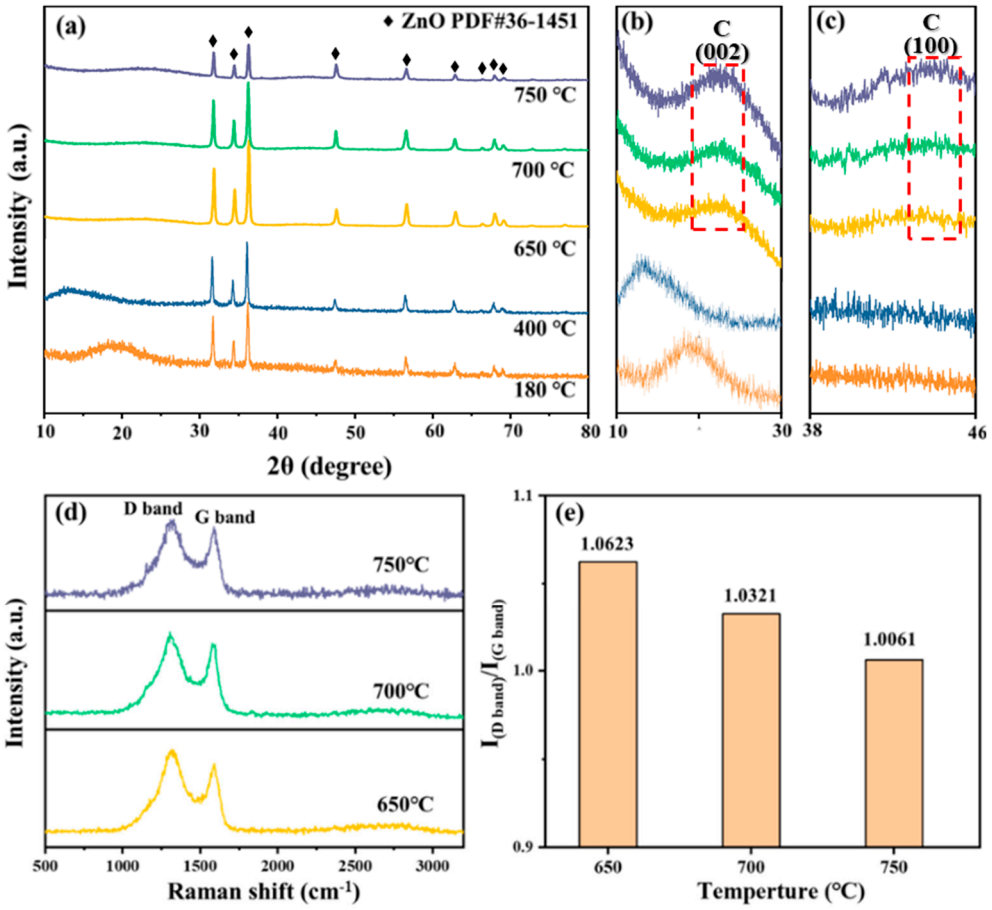

Figure 3. XRD patterns of the angular range from (**a**) 10°–80°, (**b**) 10°–30°, and (**c**) 38°–46°; (**d**) Raman spectra; and (**e**) the $I_{(D\ band)}/I_{(G\ band)}$ values of ZnO/C composite absorbents with different carbonization temperatures.

Raman spectroscopy of ZnO/C composite absorbents with different carbonization temperatures is shown in Figure 3d. It can be observed that the obvious D and G bands in the Raman spectrum of the samples after two-step carbonization can be observed, indicating the formation of partial graphitized structure during the process of final carbonization. It is well known that the ratio of $I_{(D\ band)}/I_{(G\ band)}$ could characterize the disorder and graphitization degrees of carbon materials, and the lower $I_{(D\ band)}/I_{(G\ band)}$ values represent fewer lattice defects and a much higher graphitization degree [24,25]. Figure 3e exhibits the $I_{(D\ band)}/I_{(G\ band)}$ values of ZnO/C composite absorbents fabricated with different carbonization temperatures. It is evident that the corresponding $I_{(D\ band)}/I_{(G\ band)}$ values of the samples with final carbonization temperatures of 650 °C, 700 °C, and 750 °C are 1.0623, 1.0321, and 1.0061, respectively. Therefore, the graphitization degree presents an increasing trend with increasing the carbonization temperature, which is consistent with the XRD results as shown in Figure 3a–c.

To further study the element composition and chemical state of the samples, XPS was carried out and the results are shown in Figure 4. The total spectra in Figure 4a illustrates the existence of Zn, O, and C elements, indicating the successful preparation of ZnO/C composite absorbents by the two-step carbonization method. As shown in Figure 4b, the peaks of 1022.15 eV and 1045.16 eV correspond to Zn $2p_{3/2}$ and Zn $2p_{1/2}$ orbits, respectively [26]. In addition, three peaks with binding energies of 284.22 eV, 285.14 eV, and 289.75 eV, corresponding to C-C bond, C-O bond, and C=O bond, can be

observed for the C 1s spectrum in Figure 4c. It is worth mentioning that the C-O and C=O bonds mainly come from the residual organic matter during the carbonization process of glucose. Moreover, the symmetrical peaks of the XPS spectrum corresponding to O 1s is observed in Figure 4d. The peak at 532.10 eV is related to the original lattice oxygen of ZnO, while the peak at 535.81 eV represents C=O bond, which is related to the chemisorption oxygen caused by surface hydroxyl groups [27].

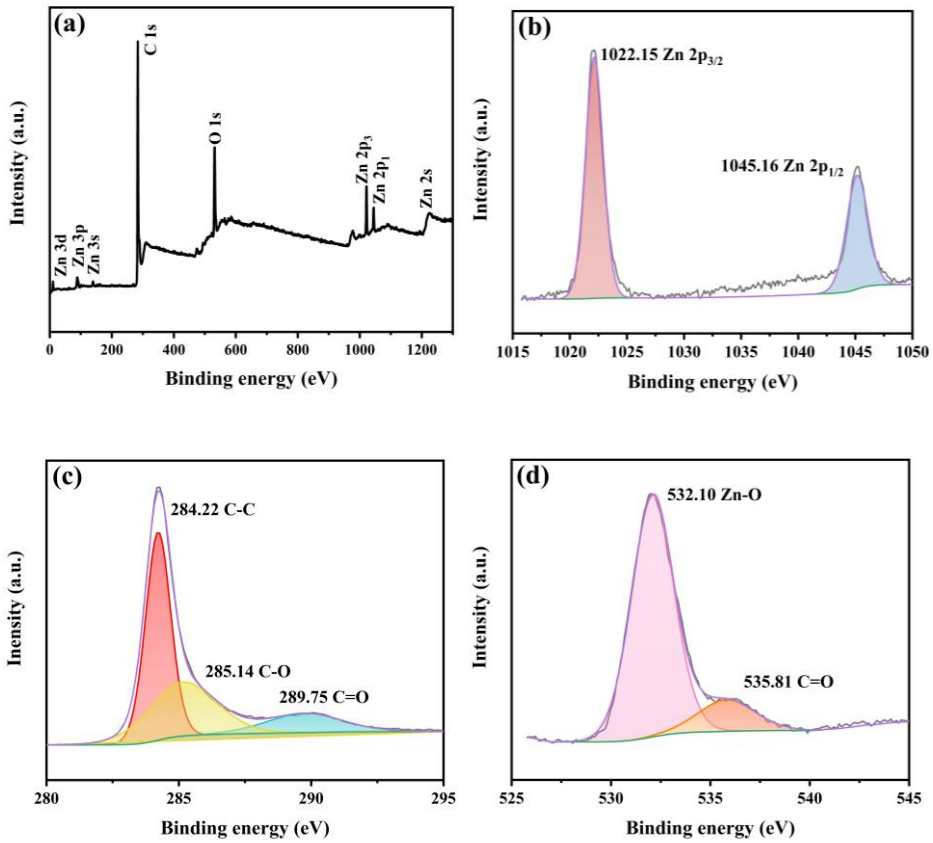

Figure 4. XPS spectrum of the sample CZO-750 (**a**) total spectra, (**b**) Zn 2p, (**c**) C 1s, (**d**) O 1s.

3.3. Surface Morphology and EDS Analysis

Figure 5 exhibits the SEM and EDS images of the prepared samples. As shown in Figure 5a, the ZnO with the length of ~2 μm and the diameter of ~0.2 μm prepared by the hydrothermal method presents a uniform rod-like structure. The carbon in the pre-carbonized ZnO/C composite absorbents exists in the form of an irregular block, and the rod-like ZnO particles are randomly distributed in the block carbon, as shown in Figure 5b,c. Because of the intensive stir of ZnO and glucose with the cohesive action of PVA solution in the preparation process, a large amount of glucose adheres to the surface of ZnO particles. However, as many more glucose molecules adhere to the ZnO surface, glucose molecules also bond with each other, resulting in the formation of large carbon blocks. In addition, it is speculated that more rod-like ZnO exists in flake carbon, and thus a compact composite structure is formed.

As shown in Figure 5d–i, the SEM images of ZnO/C composite absorbents were obtained by two-step carbonization with different temperatures, and the rod-like ZnO still exists in the interior of irregular block carbon. The distribution of Zn, C, and O elements in the EDS images as observed in Figure 5j demonstrates the existence of ZnO and carbon in the ZnO/C composite absorbents. It is worth noting that the O element was distributed in the whole image of the scanned surface, indicating the existence of many oxygen-containing functional groups in ZnO/C composite absorbents, and it is consistent with the analysis results of XPS spectrum, as shown in Figure 4.

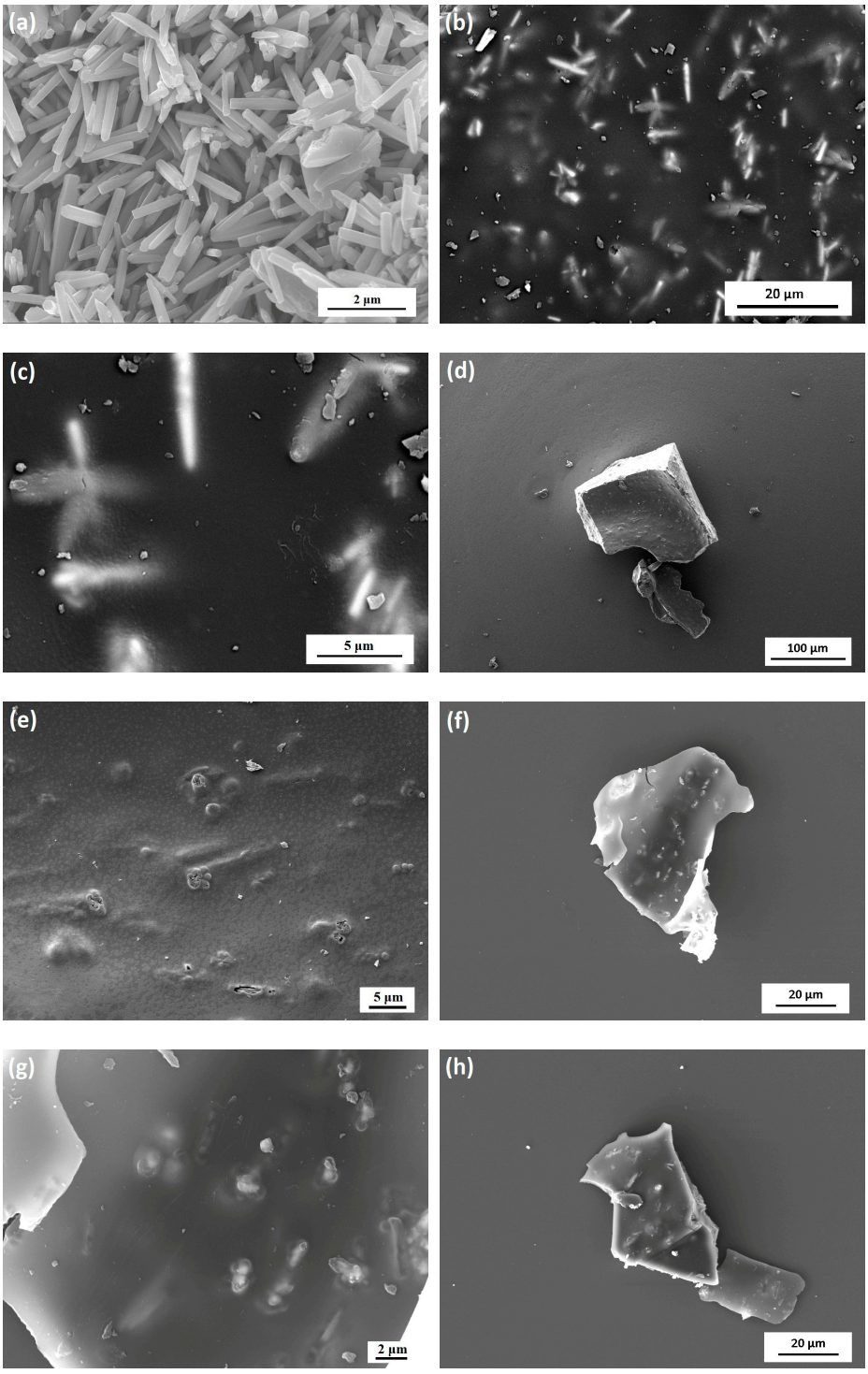

Figure 5. *Cont.*

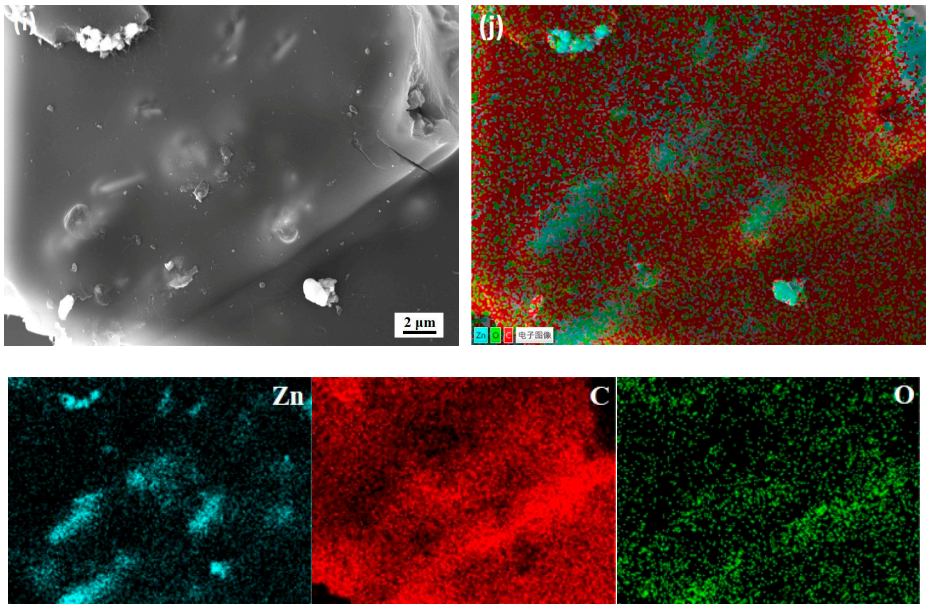

Figure 5. SEM images of the samples of (**a**) pure ZnO (**b**,**c**) PZO, (**d**,**e**) CZO-650, (**f**,**g**) CZO-700, and (**h**,**i**) CZO-750; (**j**) EDS images of the CZO-750.

3.4. Complex Permittivity and Electrical Conductivity

Figure 6 shows the curves of complex permittivity and loss tangent ($\tan\delta_\varepsilon$) of ZnO/C-filled paraffin composite samples with frequency at different carbonization temperatures and ZnO/C absorbent content. As shown in Figure 6a,b, as the temperature increases from 650 °C to 700 °C and 750 °C, the real part values of complex permittivity are in the range of 9.71–10.23, 12.78–13.22, and 15.35–16.16, while the imaginary part values of the corresponding complex permittivity are in the range of 0.72–0.94, 0.84–1.47, and 4.04–4.49, respectively. The real and imaginary parts of complex permittivity increase evidently with the increase in carbonization temperature from 650 °C to 750 °C. Figure S1 in the attachment shows the complex permittivity of the samples after curing treatment at 180 °C and pre-carbonization treatment at 400 °C. The complex permittivity of the samples without two-step carbonization is quite low, which is almost close to the complex permittivity of the paraffin. Therefore, the precursor without carbonization treatment presents poor microwave absorption properties. Figure 6d,e shows the complex permittivity of carbon-filled paraffin composite samples or ZnO/C-filled paraffin composite samples with different C or ZnO/C absorbent content. Interestingly, although the complex permittivity of ZnO-filled paraffin composite sample (as shown in Figure S2) is much lower, the complex permittivity of ZnO/C-filled paraffin composite samples is significantly improved. In addition, the $\tan\delta_\varepsilon$ values of the samples are calculated according to the complex permittivity of ZnO/C-filled paraffin composite samples and C-filled paraffin composite samples, which are presented in Figure 6c,f. It can be observed that the $\tan\delta_\varepsilon$ of the samples increases with the increase in the final carbonization temperature and the ZnO/C absorbent content.

Figure 7a shows the DC conductivity as the final carbonization temperature of ZnO/C-filled paraffin composite samples are 650 °C, 700 °C and 750 °C. With the increase in the final carbonization temperature, the DC conductivity curve of the samples shows an upward trend, which is ascribed to the increased graphitization degree of carbon products. In addition, it can be seen from Figure 7b that the DC conductivity increases with increasing ZnO/C absorbent content, and the DC conductivity of C-filled paraffin composite samples is significantly higher than those of ZnO/C-filled paraffin composite samples. As is known to all, the increase in DC conductivity could significantly improve the conductance loss ability and thus enhance their microwave absorption properties [28,29]. Therefore, the increase in graphitization degree and ZnO/C absorbent content obviously affects the DC

conductivity of the samples, playing an important role in regulating their microwave absorption properties.

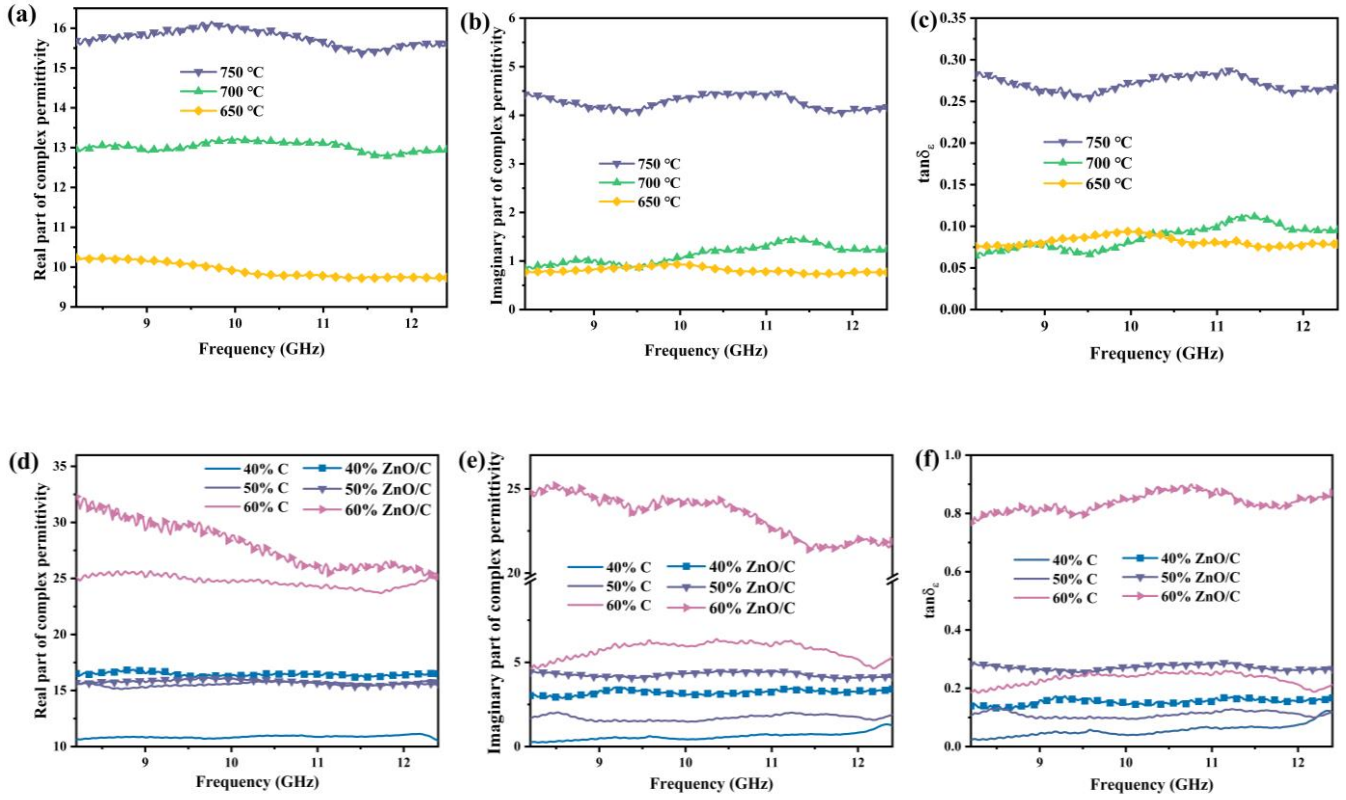

Figure 6. (**a**,**b**) Complex permittivity and (**c**) tanδ_ε of ZnO/C-filled paraffin composite samples (50 wt% ZnO/C absorbent content) with different carbonization temperatures; (**d**,**e**) complex permittivity and (**f**) tanδ_ε of ZnO/C (C)-filled paraffin composite samples (750 °C final carbonization temperature) with different C or ZnO/C absorbent content.

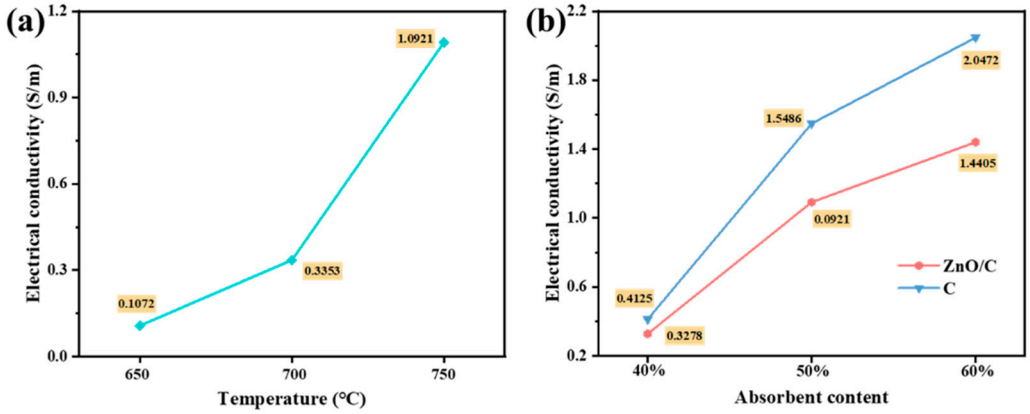

Figure 7. DC conductivity of (**a**) ZnO/C-filled paraffin composite samples (50 wt% ZnO/C absorbent content) with different carbonization temperatures and (**b**) ZnO/C (C)-filled paraffin composite samples (750 °C final carbonization temperature) with different C or ZnO/C absorbent content.

3.5. Microwave Absorption Properties

According to the transmission line theory, the reflection loss of ZnO/C (C)-filled paraffin composite samples can be calculated. The reflection loss is given by the following relationships [30]:

$$Z_{in} = Z_0(\mu_r/\varepsilon_r)^{1/2}\tanh[j(2\pi fd/c)(\mu_r\varepsilon_r)^{1/2}] \quad (2)$$

$$RL = 20\lg|(Z_{in} - Z_0)/(Z_{in} + Z_0)| \quad (3)$$

where Z_{in} and Z_0 (Z_0 = 377 Ω) are the input impedance and the impedance of free space. The μ_r ($\mu_r = \mu' - i\mu''$) and the ε_r ($\varepsilon_r = \varepsilon' - i\varepsilon''$) indicate the complex permeability and the complex permittivity, respectively [31]; f is the frequency; d is the thickness; c is the speed of light in vacuum (3×10^8 m/s).

Figure 8a–c exhibits the calculated reflection loss of ZnO/C-filled paraffin composite samples with different final carbonization temperatures. As shown in Figure 8a, the microwave absorption performance of the sample is poor when the carbonization temperature is 650 °C. As the carbonization temperature increases to 700 °C, the minimum reflection loss reaches −5.50 dB (d = 1.8 mm) in 11.46 GHz, which is exhibited in Figure 8b. By comparison, the reflection loss achieves −25.64 dB (d = 1.8 mm) and the corresponding effective absorption bandwidth reaches 2.21 GHz in 9.64–11.85 GHz when the carbonization temperature reaches 750 °C, as shown in Figure 8c. From the 3D mapping surface in Figure 8d, it can be observed that the frequency corresponding to the optimal reflection loss moves to a lower frequency region with increasing the sample thickness. This phenomenon can be illustrated by quarter wavelength theory, and the corresponding formula is given as follows [27]:

$$t_m = \frac{nc}{4f_m\sqrt{\mu_r\varepsilon_r}}(n = 1, 3, 5, \ldots) \quad (4)$$

where t_m is the matching thickness, c is the vacuum velocity, and f_m is the matching frequency. As can be seen form Formula (4), the matching thickness and the matching frequency presents the opposite trend. Figure 8c,e,f presents the reflection loss of the samples filled with 40 wt.%, 50 wt.%, and 60 wt.% ZnO/C absorbent content. Compared with the sample with 40 wt.% and 60 wt.% ZnO/C absorbent content, the ZnO/C-filled paraffin composite sample filled with 50 wt.% absorbent content presents the favorable reflection loss of −25.64 dB and optimal effective absorption bandwidth of 2.21 GHz. Table 2 exhibits the microwave absorption properties of ZnO/C composite absorbent and some other reported composites filled with ZnO or C absorbents [32–40]. In contrast, the investigated ZnO/C composite absorbent in this work presents favorable microwave absorption properties.

Impedance matching and attenuation coefficient are important parameters in evaluating microwave absorption properties of the investigated microwave absorption materials. The impedance matching ($|Z| = |Z_{in}|/Z_0$) with different carbonization temperature and ZnO/C absorbent content calculated by Formula (2) is shown in Figure 9a,c, and the favorable impedance-matching values appear in $|Z| = 1$ (black line in Figure 9a,c). As shown in Figure 9a, the impedance matching of ZnO/C-filled paraffin composite samples presents a decreasing trend with the final carbonization temperature increases from 650 °C to 700 °C and 750 °C, and the corresponding values vary in the range of 0.82–5.10, 0.66–3.72, and 0.64–1.20, respectively. Compared with ZnO/C-filled paraffin composite samples with 40 wt.% and 60 wt.% ZnO/C absorbent content, the sample filled with 50 wt.% ZnO/C absorbent content shows the most favorable impedance matching, as shown in Figure 9c. In addition, the attenuation coefficient is used to evaluate the attenuation ability of the material, and the higher attenuation coefficient represents the stronger attenuation ability [41,42]. The calculating formula of the attenuation coefficient is given as follows [39]:

$$\alpha = \frac{\sqrt{2}\pi f}{c} \times \sqrt{(\mu''\varepsilon'' - \mu'\varepsilon')^2 + \sqrt{(\mu''\varepsilon' + \mu'\varepsilon'')^2}} \quad (5)$$

Figure 9b,d present the attenuation coefficient of ZnO/C-filled paraffin composite samples with different carbonization temperature and ZnO/C absorbent content, respectively. As shown in Figure 9b,d, the attenuation coefficient increases continuously with the increase in carbonization temperature and ZnO/C absorbent content, and the sample CZO60-750 presents the highest attenuation coefficient. Based on the above comprehensive

analysis of the impedance matching and attenuation coefficient, the sample with final carbonization temperature of 750 °C and 50 wt.% absorbent content exhibits the most favorable reflection loss due to its excellent impedance-matching characteristic and favorable microwave attenuation ability.

The schematic diagram of microwave absorption mechanisms of ZnO/C-filled paraffin composite samples is shown in Figure 10. Firstly, the conductive network structure increases the conductance loss of the investigated ZnO/C composite absorbents [43]. In addition, ZnO and C form dielectric-conductivity coupling structure, the dipole polarization effect of ZnO and the interfacial polarization effect among ZnO, carbon, and paraffin greatly improve the microwave absorption properties. Furthermore, the multiple reflection of electromagnetic waves among different absorbents furtherly promotes the loss capability of the incident electromagnetic waves [44]. Finally, a unique micro capacitor structure comprised of lots of parallel plates appears in the ZnO/C composite absorbent, which enhances the loss capability. Generally, the excellent microwave absorption properties of the investigated ZnO/C composite absorbents come from the combined action of dipole polarization, conductance loss, interface polarization, and multiple reflection.

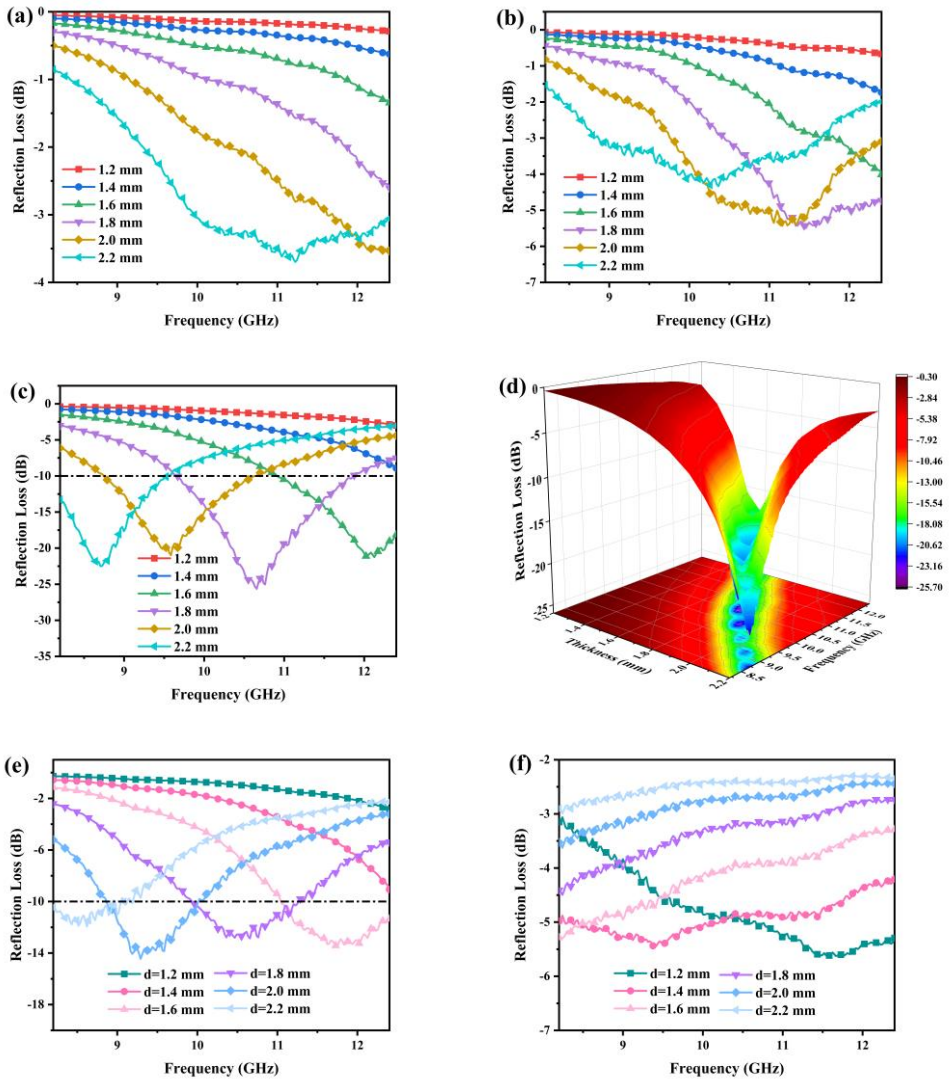

Figure 8. The variation curve of reflection loss with frequency for ZnO/C−filled paraffin composite samples of (**a**) CZO50−650, (**b**) CZO50−700, (**c**) CZO50−750, (**d**) 3D mapping surface of CZO50−750, (**e**) CZO40−750, and (**f**) CZO60−750.

Table 2. Microwave absorption properties of ZnO/C composite absorbent and some other reported composites filled with ZnO or C absorbents.

Materials	Thickness/mm	The Minimum Reflection Loss/Db	Bandwidth (<−10 Db)/GHz	Ref.
Carbon fibers	2.50	−49.4	10.8	[32]
Graphene	3.00	−4.30	4.32	[33]
CNT	2.00	−47.70	1.7	[34]
3D carbon aerogel	2.50	−41.00	5.24	[35]
PEG@CMF/rGO/MoS_2	2.10	−32.49	6.16	[36]
ZnO	3.10	−7.00	0	[37]
ZnO/Ni	3.00	−12.86	—	[38]
ZnO/$BaFe_{12}O_{19}$	4.50	−48.60	2.30	[39]
Fe_3O_4@ZnO/RGO	4.50	−34.00	~2.00	[40]
ZnO/C	1.80	−25.64	2.21	This work

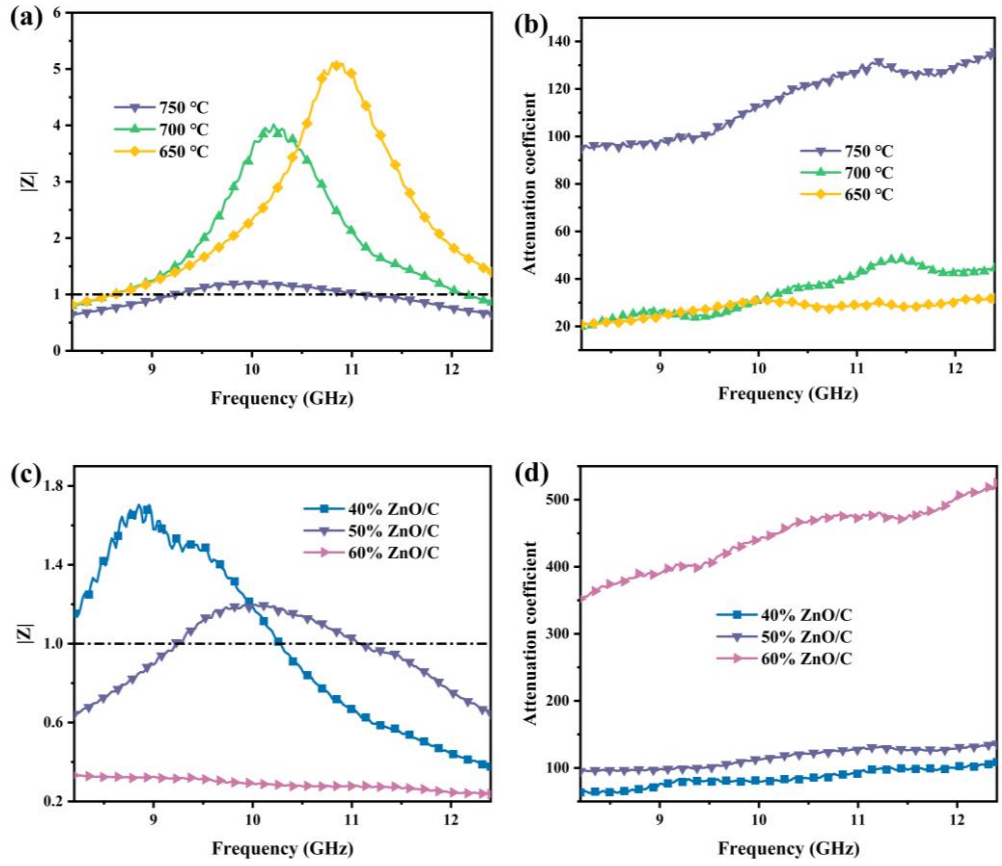

Figure 9. (**a**) Impedance matching and (**b**) attenuation coefficient curves of ZnO/C-filled paraffin composite samples (50 wt% ZnO/C absorbent content) with different carbonization temperatures; (**c**) impedance matching and (**d**) attenuation coefficient curves of ZnO/C-filled paraffin composite samples (750 °C final carbonization temperature) with different ZnO/C absorbent content.

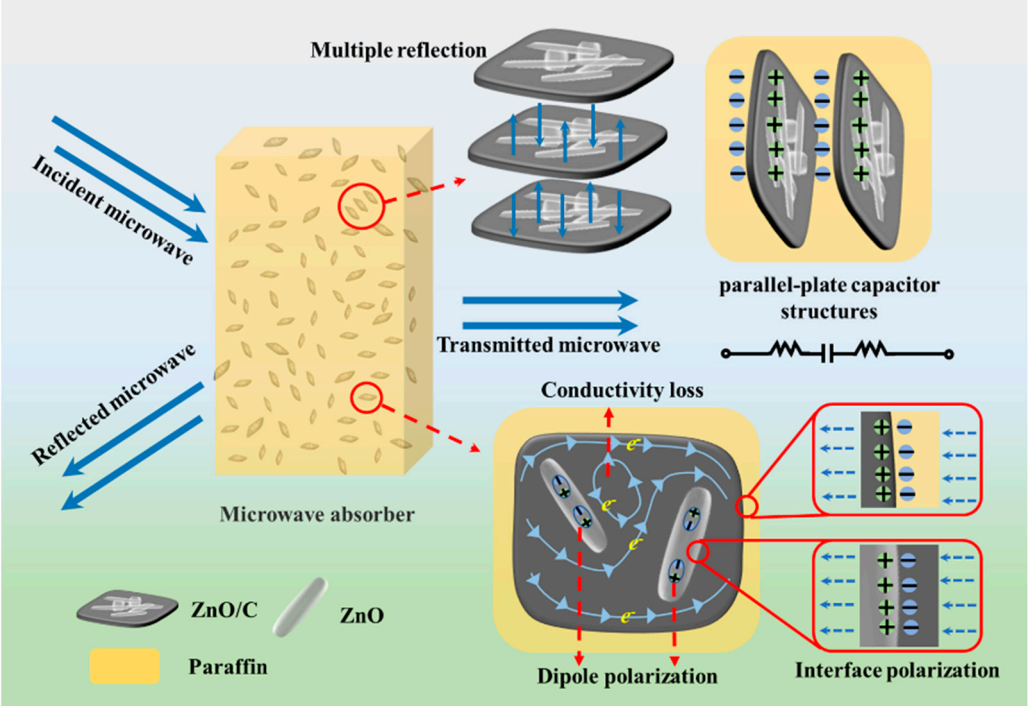

Figure 10. Schematic illustration for microwave absorption mechanisms of ZnO/C-filled paraffin composite samples.

4. Conclusions

In summary, ZnO/C composite absorbents were prepared by a two-step carbonization method, and the regulation mechanism of the final carbonization temperature on the microwave absorption properties of ZnO/C composite absorbents was studied. The dielectric-conductive coupling structure composed of ZnO and C leads to the enhancement of interface polarization, which greatly increases the microwave absorption properties. Compared with other samples, ZnO/C-filled paraffin composite samples with final carbonization temperature of 750 °C and 50 wt.% absorbent content presents the appropriate complex permittivity, excellent impedance-matching characteristic, and favorable attenuation ability, indicating the impressive microwave absorption properties with a minimum reflection loss of −25.64 dB (d = 1.8 mm) and the maximum effective bandwidth of 2.21 GHz (RL < −10 dB, 9.64–11.85 GHz). This study shows that the composite comprised of dielectric absorbent and conductive absorbent can hopefully effectively control the impedance-matching characteristic and microwave attenuation ability, which is significant for the purposeful design of superior microwave-absorbing materials with dielectric and conductive absorbents.

Supplementary Materials: The following supporting information can be downloaded at: https://www.mdpi.com/article/10.3390/met13071220/s1, Figure S1: Complex permittivity of the samples after curing treatment at 180 °C and pre-carbonization treatment at 400 °C. Figure S2: Complex permittivity of ZnO-filled paraffin composite sample.

Author Contributions: Conceptualization, H.J.; methodology, H.J.; validation, H.J., L.Z. and H.W.; formal analysis, H.W.; investigation, J.Y.; resources, L.Z. and Z.W.; data curation, J.Y.; writing—original draft preparation, J.Y.; writing—review and editing, L.Z.; visualization, J.Y.; supervision, H.J., L.Z. and Z.W.; project administration, L.Z.; funding acquisition, L.Z. All authors have read and agreed to the published version of the manuscript.

Funding: This research was funded by [Key Research and Development Program in Shaanxi Province of China] grant number [2021GY-244] and [Fundamental Research Funds for the Central Universities from Chang'an University] grant number [300102313201].

Data Availability Statement: Not applicable.

Conflicts of Interest: The authors declare no conflict of interest.

References

1. Micheli, D.; Vricella, A.; Pastore, R.; Marchetti, M. Synthesis and electromagnetic characterization of frequency selective radar absorbing materials using carbon nanopowders. *Carbon* **2014**, *77*, 756–774. [CrossRef]
2. Gupta, S.; Tai, N.H. Carbon materials and their composites for electromagnetic interference shielding effectiveness in X-band. *Carbon* **2019**, *152*, 159–187. [CrossRef]
3. Zeng, X.; Cheng, X.; Yu, R.; Stucky, G.D. Electromagnetic microwave absorption theory and recent achievements in microwave absorbers. *Carbon* **2020**, *168*, 606–623. [CrossRef]
4. Wang, Z.; Cheng, Z.; Fang, C.; Hou, X.; Xie, L. Recent advances in MXenes composites for electromagnetic interference shielding and microwave absorption. *Compos. Part A Appl. Sci. Manuf.* **2020**, *136*, 105956. [CrossRef]
5. Zhang, Z.; Cai, Z.; Wang, Z.; Peng, Y.; Xia, L.; Ma, S.; Yin, Z.; Huang, Y. A Review on Metal–Organic Framework-Derived Porous Carbon-Based Novel Microwave Absorption Materials. *Nano-Micro Lett.* **2021**, *13*, 56. [CrossRef] [PubMed]
6. Kuang, B.; Song, W.; Ning, M.; Li, J.; Zhao, Z.; Guo, D.; Cao, M.; Jin, H. Chemical reduction dependent dielectric properties and dielectric loss mechanism of reduced graphene oxide. *Carbon* **2018**, *127*, 209–217. [CrossRef]
7. Ren, Y.-L.; Wu, H.-Y.; Lu, M.-M.; Chen, Y.-J.; Zhu, C.-L.; Gao, P.; Cao, M.-S.; Li, C.-Y.; Ouyang, Q.-Y. Quaternary Nanocomposites Consisting of Graphene, Fe_3O_4@Fe Core@Shell, and ZnO Nanoparticles: Synthesis and Excellent Electromagnetic Absorption Properties. *ACS Appl. Mater. Interfaces* **2012**, *4*, 6436–6442. [CrossRef]
8. Wang, B.; Wu, Q.; Fu, Y.; Liu, T. A review on carbon/magnetic metal composites for microwave absorption. *J. Mater. Sci. Technol.* **2021**, *86*, 91–109. [CrossRef]
9. Wu, N.; Hu, Q.; Wei, R.; Mai, X.; Naik, N.; Pan, D.; Guo, Z.; Shi, Z. Review on the electromagnetic interference shielding properties of carbon based materials and their novel composites: Recent progress, challenges and prospects. *Carbon* **2021**, *176*, 88–105. [CrossRef]
10. Park, J.-H.; Lee, S.; Ro, J.C.; Suh, S.-J. Yolk–shell Fe–Fe3O4@C nanoparticles with excellent reflection loss and wide bandwidth as electromagnetic wave absorbers in the high-frequency band. *Appl. Surf. Sci.* **2021**, *573*, 151469. [CrossRef]
11. Xu, J.; Sun, L.; Qi, X.; Wang, Z.; Fu, Q.; Pan, C. A novel strategy to enhance the multiple interface effect using amorphous carbon packaged hydrogenated TiO_2 for stable and effective microwave absorption. *J. Mater. Chem. C* **2019**, *7*, 6152–6160. [CrossRef]
12. Qiang, R.; Feng, S.; Chen, Y.; Ma, Q.; Chen, B. Recent progress in biomass-derived carbonaceous composites for enhanced microwave absorption. *J. Colloid Interface Sci.* **2022**, *606*, 406–423. [CrossRef] [PubMed]
13. Zhang, D.; Liu, T.; Cheng, J.; Chai, J.; Yang, X.; Wang, H.; Zheng, G.; Cao, M. Light-weight and low-cost electromagnetic wave absorbers with high performances based on biomass-derived reduced graphene oxides. *Nanotechnology* **2019**, *30*, 445708. [CrossRef] [PubMed]
14. Zhao, H.; Cheng, Y.; Liu, W.; Yang, L.; Zhang, B.; Wang, L.P.; Ji, G.; Xu, Z.J. Biomass-Derived Porous Carbon-Based Nanostructures for Microwave Absorption. *Nano-Micro Lett.* **2019**, *11*, 24. [CrossRef]
15. Wang, X.; Bao, X.; Zhou, X.; Shi, G. Excellent microwave absorption of lamellar LaOCl/C nanocomposites with LaOCl nanoparticles embedded in carbon matrix. *J. Alloy. Compd.* **2018**, *764*, 701–708. [CrossRef]
16. Wu, H.; Wang, L.D.; Wu, H.J. Synthesis, Characterization and Microwave Absorption Properties of Dendrite-Like Fe_3O_4 Embedded within Amorphous Sugar Carbon Matrix. *Appl. Surf. Sci.* **2014**, *290*, 388–397. [CrossRef]
17. Sedlak, J.; Kuritka, I.; Masar, M.; Machovsky, M.; Urbanek, P.; Bazant, P.; Janota, P.; Dvorackova, M. Contributions of morphological and structural parameters at different hierarchical morphology levels to photocatalytic activity of mesoporous nanostructured ZnO. *Appl. Surf. Sci.* **2020**, *513*, 145773. [CrossRef]
18. Feng, W.; Wang, Y.; Chen, J.; Wang, L.; Guo, L.; Ouyang, J.; Jia, D.; Zhou, Y. Reduced graphene oxide decorated with in-situ growing ZnO nanocrystals: Facile synthesis and enhanced microwave absorption properties. *Carbon* **2016**, *108*, 52–60. [CrossRef]
19. Gao, P.X.; Wang, Z.L. Mesoporous Polyhedral Cages and Shells Formed by Textured Self-Assembly of ZnO Nanocrystals. *J. Am. Chem. Soc.* **2003**, *125*, 11299–11305. [CrossRef]
20. Araújo, J.V.; Ferreira, R.V.; Yoshida, M.I.; Pasa, V.M. Zinc nanowires synthesized on a large scale by a simple carbothermal process. *Solid State Sci.* **2009**, *11*, 1673–1679. [CrossRef]
21. He, H.K.; Gao, C. Supraparamagnetic, Conductive, and Processable Multifunctional Graphene Nanosheets Coated with High-Density Fe3O4 Nanoparticles. *ACS Appl. Mater. Inter.* **2010**, *2*, 3201–3210. [CrossRef]
22. Zeng, Q.; Xiong, X.H.; Chen, P.; Yu, Q.; Wang, Q.; Wang, R.C.; Chu, H.R. Air@rGO€Fe3O4 Microspheres with Spongy Shells: Self-Assembly and Microwave Absorption Performance. *J. Mater. Chem. C* **2016**, *4*, 10518–10528. [CrossRef]
23. Kang, S.; Zhang, W.; Hu, Z.M.; Yu, J.R.; Wang, Y.; Zhu, J. Porous Core-Shell Zeolitic Imidazolate Framework-Derived Co/NPC@ZnO-Decorated Reduced Graphene Oxide for Lightweight and Broadband Electromagnetic Wave Absorber. *J. Alloy. Compd.* **2020**, *818*, 152932. [CrossRef]
24. Sandra, V.R.; Enrique, G.B.; Lavier, H.F.; Jose, G.D.; Alejandro, A.C.; Silva, A.M.; Maser, W.K.; Benito, A.M. Controlling the Surface Chemistry of Graphene Oxide: Key Towards Efficient ZnO-GO Photocatalysts. *Catal. Today* **2020**, *357*, 350–360.

25. Liu, Y.; Du, X.M.; Wu, C.Y.; Liu, Y.N.; Liu, Y.Q.; Zhao, G.Z. Reduced Graphene Oxide Decorated with ZnO Microrods for Efficient Electromagnetic Wave Absorption Performance. *J. Mater. Sci.* **2020**, *31*, 8637–8648. [CrossRef]
26. Yuan, Y.; Qu, Z.M.; Wang, Q.G.; Sun, X.N.; Cheng, E. Reversible Nonlinear I-V Behavior of ZnO-Decorated Graphene Nanoplatelets/Epoxy Resin Composites. *Polymers* **2020**, *12*, 951–964. [CrossRef]
27. He, M.; Zhou, Y.; Huang, T.; Nie, S.; Wang, Y.; Xu, Z.; Huo, Y.; Xu, R.; Chen, X.; Peng, H. Flower-like CoS hierarchitectures@polyaniline organic-inorganic heterostructured composites: Preparation and enhanced microwave absorption performance. *Compos. Sci. Technol.* **2020**, *200*, 108403. [CrossRef]
28. Tao, J.; Zhou, J.; Yao, Z.; Jiao, Z.; Wei, B.; Tan, R.; Li, Z. Multi-shell hollow porous carbon nanoparticles with excellent microwave absorption properties. *Carbon* **2020**, *172*, 542–555. [CrossRef]
29. Wang, X.-X.; Ma, T.; Shu, J.-C.; Cao, M.-S. Confinedly tailoring Fe3O4 clusters-NG to tune electromagnetic parameters and microwave absorption with broadened bandwidth. *Chem. Eng. J.* **2018**, *332*, 321–330. [CrossRef]
30. Wang, G.; Gao, Z.; Tang, S.; Chen, C.; Duan, F.; Zhao, S.; Lin, S.; Feng, Y.; Zhou, L.; Qin, Y. Microwave Absorption Properties of Carbon Nanocoils Coated with Highly Controlled Magnetic Materials by Atomic Layer Deposition. *ACS Nano* **2012**, *6*, 11009–11017. [CrossRef] [PubMed]
31. Tan, R.Y.; Zhou, F.K.; Chen, P.; Zhang, B.S.; Zhou, J.T. PANI/FeCo@C Composite Microspheres with Broadband Microwave Absorption Performance. *Compos. Sci. Technol.* **2022**, *218*, 109143. [CrossRef]
32. Chen, J.; Wang, Y.; Liu, Y.; Tan, Y.; Zhang, J.; Liu, P.; Kong, J. Fabrication of macroporous magnetic carbon fibers via the cooperative etching-electrospinning technology toward ultra-light microwave absorption. *Carbon* **2023**, *208*, 82–91. [CrossRef]
33. Shen, X.; Ran, K.; Zheng, B.; Chen, F. Structure engineering of 3D interconnect graphene nanocapsules for microwave absorption. *Inorg. Chem. Commun.* **2023**, *153*, 110863. [CrossRef]
34. Sun, H.; Che, R.; You, X.; Jiang, Y.; Yang, Z.; Deng, J.; Qiu, L.; Peng, H. Cross-Stacking Aligned Carbon-Nanotube Films to Tune Microwave Absorption Frequencies and Increase Absorption Intensities. *Adv. Mater.* **2014**, *26*, 8120–8125. [CrossRef] [PubMed]
35. Xu, J. Three dimensional carbon aerogel for microwave absorption from chitosan. *Synth. Met.* **2023**, *295*, 117352. [CrossRef]
36. Hu, Z.; Jiang, M.; Zou, Y.; Sun, L.; Xu, F.; Yu, S.; Hao, S.; Xiang, C. MoS2-decorated carbonized melamine foam/reduced graphene oxide network for constructing polyethylene-glycol-based multifunctional phase change materials toward multiple energy harvesting and microwave absorbing applications. *Chem. Eng. J.* **2023**, *461*, 141923. [CrossRef]
37. Liu, L.; Kuang, D.; Hou, L.; Luo, H.; Deng, L.; Wang, S. Synthesis and microwave absorption performance of layered hard carbon embedded with ZnO nanoparticles. *J. Alloy. Compd.* **2021**, *895*, 162677. [CrossRef]
38. Singh, S.; Singh, S.K.; Singh, R.; Kumar, A.; Nigam, A. Effect of Ni on the Dielectric Behavior and Microwave Absorption Performance of ZnO Composites. *Mater. Phys. Mech.* **2021**, *47*, 416–422.
39. Lin, Y.; Dong, J.; Liu, Y.; Han, N.; Wang, L.; Yang, H.; Wang, J. Three-Dimensional Network ZnO/BaFe12O19 Composite Thick Films and Their Microwave Absorption Properties. *J. Ceram. Sci. Technol.* **2018**, *9*, 183–192.
40. Wang, Y.; Peng, Z.; Jiao, Y.; Jiang, W. Synthesis of Fe_3O_4@ZnO/RGO nanocomposites and microwave absorption properties. In Proceedings of the 2015 IEEE 15th International Conference on Nanotechnology (IEEE-NANO), Rome, Italy, 27–30 July 2015; pp. 220–224. [CrossRef]
41. Meng, F.; Wang, H.; Huang, F.; Guo, Y.; Wang, Z.; Hui, D.; Zhou, Z. Graphene-based microwave absorbing composites: A review and prospective. *Compos. Part B Eng.* **2018**, *137*, 260–277. [CrossRef]
42. Zhang, N.; Chen, P.; Wang, Y.; Zong, M.; Chen, W. Supramolecular self-assembly derived Mo2C/FeCo/NC hierarchical nanostructures with excellent wideband microwave absorption properties. *Compos. Sci. Technol.* **2022**, *221*, 109325. [CrossRef]
43. Wu, Q.L.; Wang, J.; Jin, H.H.; Dong, Y.W.; Huo, S.Q.; Yang, S.; Su, X.G.; Zhang, B. Facile Synthesis of Co-Embedded Porous Spherical Carbon Composites Derived from Co3O4/ZiF-8 Compounds for Broadband Microwave Absorption. *Compos. Sci. Technol.* **2020**, *195*, 108206. [CrossRef]
44. Rehman, S.U.; Wang, J.; Luo, Q.; Sun, M.; Jiang, L.; Han, Q.; Liu, J.; Bi, H. Starfish-like C/CoNiO2 heterostructure derived from ZIF-67 with tunable microwave absorption properties. *Chem. Eng. J.* **2019**, *373*, 122–130. [CrossRef]

Disclaimer/Publisher's Note: The statements, opinions and data contained in all publications are solely those of the individual author(s) and contributor(s) and not of MDPI and/or the editor(s). MDPI and/or the editor(s) disclaim responsibility for any injury to people or property resulting from any ideas, methods, instructions or products referred to in the content.